Journal of the Meteorological Society of Japan

## EARLY ONLINE RELEASE



The DOI for this manuscript is

DOI:10.2151/jmsj.2025-001

J-STAGE Advance published date: October 21, 2024

# Summertime Convection Jump over the Subtropical Western North Pacific and its Relation to Rossby Wave Breaking Near the Asian Jet Exit Region

**Ryouta NAKANISHI**[1]

*Graduate School of Science and Technology*
*University of Tsukuba, Tsukuba, Japan*

**Masaya KURAMOCHI**

*Graduate School of Science and Technology*
*University of Tsukuba, Tsukuba, Japan*
*Japan Meteorological Agency, Tokyo, Japan*

**and**

**Hiroaki UEDA**

*Faculty of Life and Environmental Sciences*
*University of Tsukuba, Tsukuba, Japan*

Manuscript received October 6, 2024

-----------------------------------

1) Corresponding author: Ryouta Nakanishi, Graduate School of Science and Technology, University of Tsukuba, 1-1-1 Tennodai, Tsukuba, Ibaraki, 305-8572, Japan
Email: s2321139@u.tsukuba.ac.jp

## Abstract

Abrupt enhancement of convective activity over the subtropical western North Pacific around 20°N, 150°E is known as the convection jump (CJ) caused by the ocean–atmosphere coupling, which is one of the important factors inducing the end of the Baiu season in Japan. Using atmospheric reanalysis and observation data for 1974–2021, this diagnosis is made for the influences of Rossby wave propagation and breaking, high-potential vorticity (PV) intrusion, and cutoff lows over the western North Pacific on CJ occurrence.

Preceding CJ occurrence, southeastward Rossby-wave propagation is discernible along the upstream of the mid-Pacific trough in the upper troposphere, and its energy accumulates over the northeast of the CJ region. The subsequent wave breaking near the exit region of the Asian jet induces the southwestward intrusion of high-PV airmass toward the northeast of the CJ region, which is concurrent with the enhancement of convective activity. The high-PV intrusion may also be interpreted as westward-moving, upper-level cutoff lows migrating from the mid-Pacific trough. The diagnosis of Q-vector indicates that variations in the extratropical upper-tropospheric circulation induce dynamical ascent, contributing to the onset and maintenance of convective activity over the CJ region. Moreover, the PV budget analysis suggests that the persistent positive advection of PV at the edge of the high-PV intrusion nearly counterbalances the intense low-PV generation by diabatic heating associated with the CJ. These results indicate that the CJ is influenced by extratropical upper-tropospheric variations as well as the coupled atmosphere–ocean system in the subtropical western North Pacific.

**Keywords** convection jump; Rossby wave breaking; Asian monsoon; cutoff low; climate system

## 1. Introduction

Convection jump (hereafter, CJ) is an abrupt enhancement of convective activity over the subtropical western North Pacific (WNP), around 20°N, 150°E, associated with seasonal evolution in the boreal mid-summer (Ueda et al. 1995; Ueda and Yasunari 1996; Xie 2023). The CJ usually occurs in late July, corresponding to the last transition of the Asian summer monsoon, and is known as one of the key triggers of the end of the rainy season in summer (Baiu) in mainland Japan. The convective heating associated with the CJ excites the stationary Rossby waves, and a resultant anomalous anticyclone over Japan brings the abrupt termination of the Baiu season (Ueda and Yasunari 1996).

Ueda and Yasunari (1996) suggested that an essential factor for the occurrence of CJ is the tongue-shaped expansion of a warm sea surface temperature (SST) pool (>29 °C) in the subtropical WNP. Associated with the seasonal evolution of the Asian summer monsoon, this warm SST expansion is formed by weak wind speed and abundant insolation under the dominance of anticyclonic circulation. A weak temperature inversion caps the atmospheric boundary layer, maintaining the free troposphere dry (Zhou et al. 2016). The surface anticyclone and its related descent are remotely maintained by the influence of the intertropical convergence zone (ITCZ) over the east of the Philippines (Ueda et al. 2009). The combination of local warm SST and subsidence enhances the instability of the troposphere. However, the surface anticyclone and its capping effect gradually disappear in accordance with the diminishment of the ITCZ along the seasonal evolution (Ueda and

Yasunari 1996; Ueda et al. 2009). The moistening in the lower troposphere over the area with warm SST, together with the weakened suppressant effects anchored by ITCZ-origin subsidence, gives rise to rapid enhancement of convection owing to reduced atmospheric stability, which hence results in CJ occurrence (Zhou et al. 2016; Xie 2023). Based on the piecewise perpetual-SST experiment, Ueda et al. (2009) demonstrated that while the warm SST tongue is necessary to enhance the convection, this condition is not sufficient to explain the abrupt occurrence of CJ, which implies that an important role is played by atmospheric transient. Furthermore, Ueda and Yasunari (1996) pointed out that the differences in the spatial distribution of the lower-tropospheric winds and SST in the WNP during late June are responsible for the emergence of typical and atypical CJ years. Their results indicated the influence of a coupled atmosphere–ocean system in the subtropical WNP linked with the seasonal evolution of the Asian summer monsoon. However, details regarding the atmospheric transient effect, especially in the upper troposphere have not yet been explicitly clarified. A deeper understanding of the mechanisms of CJ occurrence may be expected to improve the accuracy of seasonal forecasts, including that of the end of the Baiu rainy season.

In recent years, it has become clear that influences from mid-to-high latitudes extend to the tropical-to-subtropical WNP through wave propagation/breaking, modulating the convective activity east of the Philippines. In particular, Takemura and Mukougawa (2020) revealed that extratropical Rossby wave breaking (RWB) near the east of Japan and associated southwestward intrusion of the high-potential vorticity (PV) airmass at the tropopause can intensify the convective activity over the subtropical WNP, which subsequently excites the Pacific–Japan teleconnection pattern. Using a $Q$-vector diagnosis, they also indicated that the enhanced convection is caused by dynamically induced ascent related to the southwestward intrusion of the high-PV airmass. Moreover, the equatorward high-PV intrusion in the upper troposphere has been shown to cause anomalous upwelling accompanied by enhanced precipitation in the tropics (Funatsu and Waugh 2008), and the formation of tropical cyclones (Galarneau et al. 2015; Fudeyasu and Yoshida 2019; Takemura and Mukougawa 2021). Although previous research on the CJ has exclusively focused on the tropical-to-subtropical regions, studying the extratropical processes may provide a new perspective on occurrence mechanisms of CJ.

In the Northern Hemisphere summer, RWB frequently occurs over the subtropical WNP, where the westerly jet is decelerated (Postel and Hitchman 1999; Abatzoglou and Magnusdottir 2006). As shown in Fig. 1a, the large-scale trough in the upper troposphere extending southwestward over the North Pacific is referred to as the mid-Pacific trough (MPT). Murakami and Matsumoto (1994) discussed the importance of the MPT and related transient perturbations on the seasonal processes of the WNP monsoon considering the interaction between the tropics and extratropics. The CJ region (purple rectangle in Fig. 1; Ueda et al. 1995) is geographically located near the southwestern edge of the MPT, which motivated us to examine the relationship between CJs and upper-tropospheric extratropical circulations (i.e., the high-PV intrusion, RWB, and MPT). Indeed, upper-level cold lows migrating westward from the MPT have been indicated to enhance convective activity near Marcus Island (Sato et al. 2005). Moreover, Lu et al. (2007) suggested a possible relationship between the CJ onset and extratropical circulation anomalies propagating westward over the North Pacific. However, the detailed physical processes of wave propagation/breaking and resultant ascent remain unrevealed. Therefore, in this study, we attempted to clarify the relationship between CJ occurrence and upper-tropospheric extratropical circulations: high-PV intrusion, Rossby wave propagation/breaking, and cutoff lows.

## 2. Data and method

This study used 6-hourly isobaric data from the Japanese 55-year reanalysis (JRA-55; Kobayashi et al. 2015), with a horizontal resolution of 1.25° and 37 pressure levels, isentropic PV data at the 360-K surface from JRA-55, and daily mean data of outgoing longwave radiation (OLR) provided by the National Oceanic and Atmospheric Administration (NOAA) with a horizontal resolution of 2.5° (Liebmann and Smith 1996) for the period of 1974–2021. To exclude noise from disturbances at a daily scale, we applied a 5-day running mean to the 6-hourly and daily data from JRA-55 and NOAA, respectively. Climatological means were obtained by averaging values for the same calendar days over the entire study period; deviations from these means were denoted as anomalies. Statistical significance of composite anomalies was assessed through the t-test with degrees of freedom based on the number of sample years.

Using the mean black body temperature, Ueda et al. (1995) showed that CJs occur in late July around the area of [15–25°N, 150–160°E], which was denoted as a key region (hereafter the CJ region; purple rectangle in Fig. 1). In this study, the definition of the CJ region is geographically fixed following to the previous studies. CJ day was defined as the day when 5-day running mean OLR averaged in the CJ region was below 200 W $m^{-2}$ and reached a minimum in the period between July 20 and August 8 of individual years. Twenty CJ days were identified, which are listed in Table 1. We call years with (without) the CJ day as typical (atypical) CJ years. Figures 2a and 2b show the time series of the 5-day running mean OLR from July 1 to August 10, displaying typical and atypical years, respectively. Figure 2c shows the composite time series of averaged OLR in the CJ region from 10 days before the CJ day (day −10) to 10 days after the CJ day (day +10), together with the averaged 850-hPa geopotential height anomaly in the east of Japan [35–45°N, 135–155°E]. The OLR anomalies turned from positive (i.e., suppressed) to negative (i.e., enhanced) around day −5 and kept enhancement for approximately 10 days. Significant positive anomalies of 850-hPa height after day 0 indicate the extension of the lower-tropospheric anticyclone and withdrawal of the Baiu front. In the following section, we conducted a lag composite analysis for all CJ days to clarify the variations in extratropical atmospheric circulation associated with the CJ.

We used the cutoff low index (COL index) proposed by Kasuga et al. (2021) to detect cutoff lows and preexisting troughs, seamlessly extracting them as synoptic depressions. The average slope (AS) function, one of the variables of COL index, representing the two-dimensional average of four-directional slopes, is defined as follows:

$$\mathrm{AS}(x, y; r) = \frac{1}{4r}\left[Z(x+r, y) + Z(x-r, y) + Z(x, y+r) + Z(x, y-r) - 4Z(x, y)\right], \qquad (1)$$

where $x$ and $y$ denote the longitudinal and latitudinal grid points, respectively; $r$ is the radial searching variable, and $Z$ is the geopotential height at any isobaric level. The AS maximum against variable $r$ is denoted $\mathrm{AS}^{+}$, representing depressions in the geopotential height field, and is given by:

$$\mathrm{AS}^{+}(x, y) \equiv \max_{r} \mathrm{AS}(x, y; r). \quad (2)$$

This scheme was calculated based on the 6-hourly geopotential height data at 200 hPa obtained from JRA-55.

The propagation of Rossby wave packets was analyzed using the wave-activity flux (WAF) proposed by Takaya and Nakamura (2001). The horizontal WAF is defined as follows:

$$\mathbf{W} = \frac{p^{*}}{2|\mathbf{V}|}\begin{pmatrix} U(\psi_x'^2 - \psi'\psi_{xx}') + V(\psi_x'\psi_y' - \psi'\psi_{xy}') \\ U(\psi_x'\psi_y' - \psi'\psi_{xy}') + V(\psi_y'^2 - \psi'\psi_{yy}') \end{pmatrix}, \qquad (3)$$

where $U$ is the background zonal wind, $V$ is the background meridional wind, $\mathbf{V}$ is the background horizontal wind vector, $\psi$ is the geostrophic stream function, and $p^{*}$ is the pressure normalized by 1000 hPa, with primes indicating anomalies. The background states were given by the climatological mean. The subscripts $x$ and $y$ denote the partial derivatives with respect to longitude and latitude, respectively. The flux **W** is parallel to the group velocity of the stationary Rossby waves.

The dynamical relationship between mid- to upper-tropospheric variation associated with southward intrusion of high-PV airmass and ascent over the CJ region was diagnosed using the *Q*-vectors (Hoskins et al. 1978). The *Q*-vector is given by

$$\mathbf{Q} \equiv \left(-\frac{R}{p}\frac{\partial \mathbf{v}_{\mathrm{g}}}{\partial x} \cdot \nabla T, -\frac{R}{p}\frac{\partial \mathbf{v}_{\mathrm{g}}}{\partial y} \cdot \nabla T\right), \qquad (4)$$

where $p$ represents the pressure, $\mathbf{v}_{\mathrm{g}}$ is the geostrophic horizontal wind vector, and $T$ is the temperature. The *Q*-vector form of the ω equation indicates that *Q*-vector convergence and divergence correspond to dynamically induced ascent and descent, respectively, under the quasi-geostrophic balance (Hoskins et al. 1978). The diagnosis by the *Q*-vector can quantify ascending motions induced by the upper-level dynamics rather than those by the lower-level convection-related thermodynamics. In this study, we used vertical integrated (from 850 to 200 hPa) anomalous *Q*-vector because the influence of upper-level dynamics related to the high-PV intrusion can reach the lower-level via the coupling effect (Hoskins et al. 1985).

Furthermore, we conducted a PV budget analysis to examine the role of upper-tropospheric variability on the CJ by separating the intrusion of upper-level high-PV and the generation of low-PV by anomalous convective activity. The Ertel's PV equation is as follows:

$$\frac{\partial P}{\partial t} = -\mathbf{v} \cdot \boldsymbol{\nabla}_{\theta} P + R, \qquad (5)$$

where $P$ is the PV, $\mathbf{v}$ is the horizontal wind vector, $\boldsymbol{\nabla}_{\theta}$ is the horizontal gradient operator at the potential temperature surface, and $R$ is a residual term including the diabatic heating effect and other non-conservative processes such as frictional forcing. Assuming negligible friction forcing together with large- and synoptic-scale atmospheric circulation in the free troposphere, the diabatic heating effect is dominant for $R$ and decreases PV above the heating (Hoskins and James 2014). Thus, Eq. (5) is interpreted to show that the local time tendency of PV is explained by the total amount of the PV advection and the diabatic heating effect.

## 3. Results

### *3.1 Extratropical upper-tropospheric variation related to the CJ*

Figure 3 shows composite maps of the upper-tropospheric geopotential height, PV, and $AS^+$ of the COL index on days −5, −3, −1, 0, +1, and +3 for all 20 CJ events. On day −5, the composite geopotential height, 360-K PV, and $AS^+$ fields represented the planetary-scale trough over the central North Pacific recognized as the MPT (Figs. 3a, b, c). The geopotential height field exhibits a noteworthy anticyclonic anomaly over the North Pacific (50°N, 160°E), corresponding to the upstream of the MPT (Fig. 3a), which began growing on day −7 (not shown). The WAF indicates that quasi-stationary Rossby wave packets propagated eastward and southward from the anticyclonic anomaly along the composite geopotential field (Figs. 3a, d, g, j). From day −3 to day 0, a significant cyclonic anomaly develops in the north of the CJ region, corresponding to the southwestward extension of the MPT. Simultaneously, the southward WAF emanating from the anticyclonic anomaly disappears over the cyclonic anomaly north of the CJ region, indicating the convergence of the WAF and accumulation of wave energy (Figs. 3d, g, j). This accumulated wave energy contributes to the occurrence of RWB as seen in the PV field, which shows an “inverse-S” shaped overturning from day −1 to day +3 (Figs. 3h, k, n, q). This was also evidenced in the composite geopotential height field, exhibiting a reversal of the meridional height gradient accompanied by the cyclonic anomaly in the subtropics (Figs. 3g, j, m). The high-PV airmass intruded northeast of the CJ region in association with the anticyclonic RWB (Figs. 3h, k, n, q), which may induce anomalous ascent over the CJ region (Figs. 3i, l, o, r). The negative value of the vertical *p*-velocity at 500 hPa appears to reach its peak after day 0.

The $AS^+$ of the COL index captured the simultaneity between the cyclonic anomaly intrusion associated with RWB occurrence and the reinforced convective activity over the CJ region (right column of Fig. 3). The isobaric depressions develop northeast of the CJ region from day −2 to day 0, and are maintained until day +1 (Figs. 3i, l, o). The deepening and extension of the cyclonic anomaly are related to a westward-moving cutoff low, which suggests that the westward migration of cutoff lows from the MPT partly explains the high-PV intrusion. From the perspective of PV dynamics, relatively small vortices such as cutoff lows behave as sources of same-sign PV for large-scale perturbations (Yamazaki and Itoh 2013). A recent study further suggested that cutoff lows as small-scale high-PV vorticities can contribute to form a large-scale high-PV air mass and their intrusion via the diabatic modification as well as their mergers (Yamamoto et al. 2024). As in Fig. S1, which shows the time evolution of $AS^{+}$ for the 1998 CJ event, a circle-shaped geopotential height depression, corresponding to a cutoff low, migrated westward from the central Pacific and was subsequently located around the CJ region from day −2 to day +1 (Figs. S1c–e). These results suggest that the RWB over the WNP, together with southward high-PV intrusion and westward-moving cutoff lows, is closely associated with the CJ onset.

Regarding the relationship between the high-PV intrusion and vertical motion accompanied by diabatic heating, the PV budget on the upper-level isentropic surface is assessed focusing on two effects of the advection by horizontal winds and generation by heating based on Eq. (5). As shown in Fig. 4a, positive PV advection is notably distributed at the southwestern edge of the intruding high-PV over the CJ region due to the southward winds. The positive advection persists throughout the CJ events and intensifies from day 0 to day +2 (Fig. 4b). Simultaneously, the residual term exhibits low-PV generation (green contours in Fig. 4a), corresponding to the diabatic heating effect and acts to dump the positive PV advection. The time series of the net PV tendency shows that the local tendency is almost negligible prior to day 0 owing to the balance between the advection and heating effects. However, the PV decreased slightly after the CJ from day +1 to day +3 because of the intense low-PV generation by convective heating in the mid-troposphere.

To further assess the dynamically induced vertical motion in view of the quasi-geostrophic balance on pressure coordinates, Fig. 4c shows the time series of the vertically integrated anomalous *Q*-vector divergence and 500-hPa vertical *p*-velocity averaged over the CJ region. The $Q$-vector divergence and vertical $p$-velocity vary coherently, indicating a close relationship between the intensified ascent and tropospheric circulation variation, mainly due to the southwestward intrusion of high-PV associated with the RWB. However, the mid-tropospheric ascent is enhanced from day −3, approximately reaching peaks on days +3 and +4 instead of day 0. Similarly, the anomalous $Q$-vector converges from day −1 to day +4, contributing to the anomalous ascent after day 0, when the OLR showed minimum values. This feature appears to be consistent with the maxima of high-PV advection and the diabatic heating effect after CJ occurrence (Fig. 4b) as well as the persistence of RWB from day +1 to day +3 (Figs. 3n, q). Moreover, the lag between the OLR minimum and the peak of ascent might be related to the circulation-convection feedback, indicating that the anomalous upwelling associated with convective activity may be enhanced after cloud tops reach the tropopause.

### *3.2 Comparison between typical and atypical years*

In this subsection, we compare the characteristics of upper-tropospheric circulation and tropical seasonal evolution between typical and atypical years. Owing to the absence of day 0 in atypical years (because CJ did not occur in atypical years as in Fig. 2b), composite time-mean fields for July 20–August 8 were shown as the background environment of atypical years. Based on the criteria, the 28 atypical years were defined as those excluding the typical years shown in Table 1 for the 1974–2021 period. Figure 5 shows the composite values and anomalies of the 200-hPa geopotential height in atypical years. The anomalous geopotential height field exhibits a weakening of the MPT relative to the climatology and a significant cyclonic anomaly over the North Pacific (50°N, 160°E), opposite to the corresponding anomalous anticyclone in typical years (Fig. 3). The anomalous cyclonic circulation near the Asian jet exit region indicates a southward shift of the Asian jet and eastward shift of its exit during atypical years, which are favorable for the decrease of the RWB frequency in the WNP. These results seem to affirm the role of RWB in the CJ occurrence. Takemura et al. (2020) showed that summertime the RWB frequency near Japan significantly increases during La Niña years, associated with the northward shift of the Asian jet, whereas it tends to decrease in years with an El Niño-like SST pattern. Moreover, Ueda and Yasunari (1996) indicated that most atypical years of CJ coincide with El Niño years. These results by previous studies are consistent with those obtained here, showing an important relationship with upper-tropospheric variation, specifically RWB, in both years with or without CJ occurrence.

Nevertheless, our results do not negate the importance of tropical air–sea interactions in CJ occurrence, as highlighted by previous research. We compared the tropical seasonal evolution between typical and atypical years, focusing on the variation in the ITCZ, which plays a crucial role in CJ occurrence (Ueda et al. 2009). The time series of OLR anomalies averaged in the CJ region and east of the Philippines are shown in Fig. S2a. In typical years, the ITCZ is significantly more active in early July but weakened just before the CJ period; the time series of atypical years shows a mirror image. The spatial distribution of the composite difference in OLR between typical and atypical years from June 20 to July 19 is shown in Fig. S2b. The significant negative OLR anomaly east of the Philippines indicates active convection associated with the ITCZ, suggesting its key contribution to subsequent CJ occurrence. These results support the conclusions drawn by Ueda et al. (2009) and suggest that both the coupled atmosphere–ocean system and upper-tropospheric variations can be responsible for the emergence of typical or atypical CJ years.

## 4. Summary and discussion

In this study, the relationship between CJ occurrence and extratropical upper-tropospheric circulation was examined using a lag-composite analysis, PV budget analysis, and *Q*-vector diagnosis. At CJ onset, anticyclonic RWB occurs in the Asian jet exit region from day −1 to day +3, accompanied by preceding southward Rossby-wave propagation and energy accumulation over the subtropical WNP in the upper troposphere. Simultaneously, the cyclonic anomaly develops over the northeast of the CJ region in association with southwestward high-PV intrusion. The high-PV intrusion related to the anticyclonic RWB may also be explained by the strengthening of the MPT and westward migration of the cutoff lows. The anomalous field of upper-tropospheric circulation mainly caused by the RWB promotes dynamical ascent over the CJ region from day −1 to day +3, contributing to the enhancement and maintenance of the convective activity. The convective heating locally generates a low-PV in the upper troposphere, while it tends to counterbalance the upper-level positive PV advection associated with the RWB. The anticyclonic anomaly over the northeast of the jet exit region that appeared in the typical 20 CJs is indicative of the deceleration of the Asian jet, which is suitable for the occurrence of RWB and subsequent CJ. In contrast, during atypical years, the Asian jet was anomalously accelerated, which is consistent with the absence of CJ from the perspective of RWB occurrence. Therefore, the RWB and high-PV intrusion near the Asian jet exit region play an encouraging role in the occurrence and maintenance of CJ.

Our results suggest that the atmospheric transient effect in the extratropics could also play an important role in the seasonal evolution of summer monsoon over the western North Pacific, in addition to the previously revealed coupled atmosphere–ocean systems in the tropics (Ueda and Yasunari 1996). Ueda et al. (2009) suggested the importance of atmospheric transient effects on the retreat of the lower-tropospheric anticyclone and resultant rapid CJ occurrence. The present study clarified the details of physical processes in the atmospheric transient, whose role was unknown but considered important as suggested by Ueda et al. (2009). Figure 6 summarizes the mechanisms of CJ including those shown by previous research on the tropical regions as well as those revealed in the present study. The bottom layer in Fig. 6 illustrates the maturing process of the subtropical Asian summer monsoon and the effects of SST warming on CJ onset, as indicated by previous studies. The warm SST pool and capping effect associated with the lower-tropospheric anticyclonic circulation supported by the ITCZ intensifies the instability of the troposphere over the CJ region. The retreat of the ITCZ in late July and subsequent weakening of the anticyclonic circulation trigger CJ occurrence. Meanwhile, the upper layer in Fig. 6 shows the variation in upper tropospheric circulations (RWB, high-PV intrusion, and cutoff low migration) that promote anomalous ascent and contribute to CJ occurrence, as indicated in the present study. Our study confirmed that understanding the annual march in the tropics and extratropics as well as their synchronization over the subtropical WNP toward the southwest of the MPT is important to clarify summertime seasonal evolution, including CJ emergence.

Although the present study mainly considered the one-way influence of wave breaking on CJ activation, the feedback relationship between CJ and RWB over the WNP should be considered. Upper-tropospheric divergent flows are closely associated with active convection accompanied by a large extent of latent heat and contribute to the evolution of Rossby waves and blocking by generating and poleward advection of low-PV (Teubler and Riemer 2016; Steinfeld and Pfahl 2019). Diabatic processes have also been shown to affect the intensity of cutoff lows (e.g., Wirth 1995; Portmann et al. 2018), suggesting that resultant CJ may contribute to the extratropical RWB, especially for their maintenance, and intrusion of cutoff lows. Moreover, interactive feedback might be associated with the mechanism for the systematic lag between OLR minima and vertical *p*-velocity. This should be investigated in future studies from the perspectives of cloud dynamics as well as circulation dynamics. Another important aspect is understanding the detailed process of RWB related to CJ occurrence. The triggers behind the anticyclonic anomaly over the North Pacific and RWB over the WNP derived from our composite analysis remain unclear. Takemura and Mukougawa (2020), who shifted atmospheric circulation anomalies of each case of RWB horizontally before conducting the composite analysis, suggested that Rossby wave propagation along the Asian jet and the accumulation of wave energy near the jet exit are the primary factors of wave breaking and the subsequent enhancement of convective activity. Moreover, it has been shown that the Rossby wave train along the polar front jet over northern Eurasia affects RWB over the Far East (Nakamura and Fukamachi 2004). Although the Rossby wave propagation along the Asian jet is not observed in the present study, there is a possibility that the Rossby wave propagation does occur but takes different paths in different typical CJ years that may cancel out each other in the simple composite analysis (Fig. 3). Therefore, classifying and further understanding the RWB process near the Asian jet exit region should be the focus of future studies.

Finally, CJ occurrence in the absence of extratropical assistance should be discussed. The intrusion of cutoff lows was not clearly observed in some CJ cases. Thus, further investigation is required to estimate the contribution percentage of variations in extratropical circulation to CJ occurrence. Additionally, the seasonal maturing process of the subtropical Asian monsoon and seasonal migration of the ITCZ may be related to RWB or other extratropical tropospheric transients. The tropical intra-seasonal oscillations (including the Madden–Julian oscillation and boreal summer intra-seasonal oscillation) and Indo-western

Pacific inter-basin interactions, also modulate the environmental factors affecting CJ occurrence through anomalous convective activity and SST. Although tropical and extratropical processes are both necessary conditions for CJ occurrence, subsequent research should determine how CJs are affected when these processes are synchronized or unsynchronized.

**Data Availability Statement**

The JRA-55 datasets were provided by the Japan Meteorological Agency (https://jra.kishou.go.jp/JRA-55/index_en.html), and the Interpolated OLR data were provided by NOAA PSL (https://psl.noaa.gov/).

**Supplements**

Supplement 1 shows $AS^+$ and vertical *p*-velocity in the 1998 CJ event. Supplement 2 shows a comparison of tropical seasonal evolution between the typical and atypical years focusing on the ITCZ.

**Acknowledgments**

The authors are grateful to Drs. Meiji Honda and Satoru Kasuga for providing the COL-index data and to Drs. Koutarou Takaya and Kazuto Takemura for their helpful comments and constructive discussion. We also thank two anonymous reviewers for their constructive comments and suggestions. This work was supported by the JSPS KAKENHI, grant number 23K20542. The second author (MK) was supported by the JSPS Research Fellowship for Young Scientists.

## References

Abatzoglou, J. T., and G. Magnusdottir, 2006: Planetary wave breaking and nonlinear reflection: Seasonal cycle and interannual variability. *J. Climate*, **19**, 6139−6152.

Fudeyasu, H., and R. Yoshida, 2019: Statistical analysis of the relationship between upper tropospheric cold lows and tropical cyclone genesis over the western North Pacific. *J. Meteor. Soc. Japan*, **97**, 439–451.

Funatsu, B. M., and D. W. Waugh, 2008: Connections between potential vorticity intrusions and convection in the eastern tropical Pacific. *J. Atmos. Sci.*, **65**, 987–1002.

Galarneau, T. J., R. McTaggart-Cowan, L. F. Bosart, and C. A. Davis, 2015: Development of North Atlantic tropical disturbances near upper-level potential vorticity streamers. *J. Atmos. Sci.*, **72**, 572–597.

Hoskins, B. J., I. Draghici, and H. C. Davies, 1978: A new look at the ω-equation. *Quart. J. Roy. Meteor. Soc.,* **104**, 31–38.

Hoskins, B. J., and I. N. James, 2014: *Fluid dynamics of the midlatitude atmosphere.* John Wiley & Sons, 408 pp.

Kasuga, S., M. Honda, J. Ukita, S. Yamane, H. Kawase, and A. Yamazaki, 2021: Seamless detection of cutoff lows and preexisting trough. *Mon. Wea. Rev.*, **149**, 3119–3134.

Kobayashi, S., Y. Ota, Y. Harada, A. Ebita, M. Moriya, H. Onoda, K. Onogi, H. Kamahori, C. Kobayashi, H. Endo, K. Miyaoka, and K. Takahashi, 2015: The JRA-55 reanalysis: General specifications and basic characteristics. *J. Meteor. Soc. Japan*, **93**, 5–48.

Liebmann, B., and C. A. Smith, 1996: Description of a complete (interpolated) outgoing longwave radiation dataset. *Bull. Amer. Meteor. Soc.*, **77**, 1275–1277.

Lu, R., H. Ding, C.-S. Ryu, Z. Lin, and H. Dong, 2007: Midlatitude westward propagating disturbances preceding intraseasonal oscillations of convection over the subtropical western North Pacific during summer. *Geophys. Res. Lett.*, **24**, L21702, doi:10.1029/2007GL031277.

Murakami, T., and J. Matsumoto, 1994: Summer monsoon over the Asian continent and western North Pacific. *J. Meteor. Soc. Japan*, **72**, 719–745.

Nakamura, H., and T. Fukamachi, 2004: Evolution and dynamics of summertime blocking over the Far East and the associated surface Okhotsk high. *Quart. J. Roy. Meteor. Soc.*, **130**, 1213–1233.

Portmann, R., B. Crezee, J. Quinting, and H. Wernli, 2018: The complex life cycles of two long-lived potential vorticity cut-offs over Europe. *Quart. J. Roy. Meteor. Soc.*, **144**, 701–719.

Postel, G. A., and M. H. Hitchman, 1999: A climatology of Rossby wave breaking along the subtropical tropopause. *J. Atmos. Sci.*, **56**, 359−373.

Sato, N., K. Sakamoto, and M. Takahashi, 2005: An air mass with high potential vorticity preceding the formation of the Marcus Convergence Zone. *Geophys. Res. Lett.*, **32**, L17801, doi:10.1029/2005GL023572.

Steinfeld, D. and S. Pfahl, 2019: The role of latent heating in atmospheric blocking dynamics: a global climatology. *Clim. Dyn.*, **53**, 6159–6180.

Takaya, K., and H. Nakamura, 2001: A formulation of a phase-independent wave-activity flux for stationary and migratory quasigeostrophic eddies on a zonally varying basic flow. *J. Atmos. Sci.*, **58**, 607–627.

Takemura, K., and H. Mukougawa, 2020: Dynamical relationship between quasi-stationary Rossby wave propagation along the Asian jet and Pasific-Japan pattern in boreal summer. *J. Meteor. Soc. Japan*, **98**, 169–187.

Takemura, K., and H. Mukougawa, 2021: Tropical cyclogenesis triggered by Rossby wave breaking over the western North Pacific. *SOLA*, **17**, 164–169.

Takemura, K., H. Mukougawa, and S. Maeda, 2020: Large-scale atmospheric circulation related to frequent Rossby wave breaking near Japan in boreal simmer. *J. Climate*, **33**, 6371–6744.

Teubler, F., and M. Riemer, 2016: Dynamics of Rossby wave packets in a quantitative potential vorticity–potential temperature framework. *J. Atmos. Sci.*, **73**, 1063–1081.

Ueda, H., M. Ohba, and S.-P. Xie, 2009: Important factors for the development of the Asian–Northwest Pacific summer monsoon. *J. Climate*, **22**, 649–669.

Ueda, H., and T. Yasunari, 1996: Maturing process on the summer monsoon over the western North Pacific—A coupled ocean/atmosphere system. *J. Meteor. Soc. Japan*, **74**, 493–508.

Ueda, H., T. Yasunari, and R. Kawamura, 1995: Abrupt seasonal change of large-scale convective activity over the western Pacific in the northern summer. *J. Meteor. Soc. Japan*, **73**, 795–809.

Wirth, V., 1995: Diabatic heating in an axisymmetric cut-off cyclone and related stratosphere-troposphere exchange. *Quart. J. Roy. Meteor. Soc.*, **121**, 127–147.

Xie, S.-P., 2023: *Coupled Atmosphere-Ocean Dynamics: From El Niño to Climate Change.* Elsevier Science, 424 pp.

Yamamoto, A., K. Iga, and A. Yamazaki, 2024: Mergers as the maintenance mechanism of cutoff Lows: A case study over Europe in July 2021. *Mon. Wet. Rev.*, **152**,1241–1256

Yamazaki, A., and H. Itoh, 2013: Vortex–vortex interactions for the maintenance of blocking. Part I: The selective absorption mechanism and a case study. *J. Atmos. Sci.*, **70**, 725–742.

Zhou, W., S.-P. Xie, and Z.-Q. Zhou, 2016: Slow preconditioning for the abrupt convective jump over the northwest Pacific during summer. *J. Climate*, **29**, 8103–8113.

# List of Figures

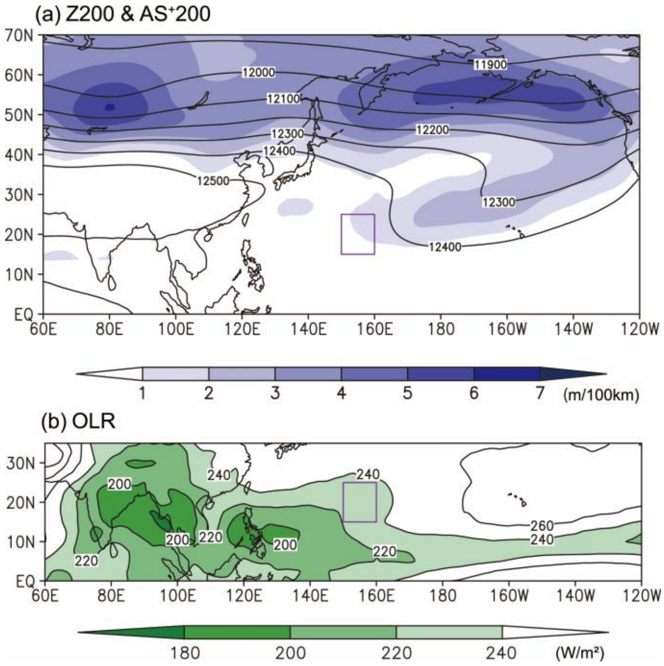


Fig. 1. Climatological mean in July 20–August 8 for the period of 1974–2021. (a) Geopotential height (contours; m) and $AS^+$ of the COL index (shading; m [100 km]$^{-1}$) at 200 hPa. (b) OLR (W m$^{-2}$). Purple rectangles indicate the CJ region [15–25°N, 150–160°E].

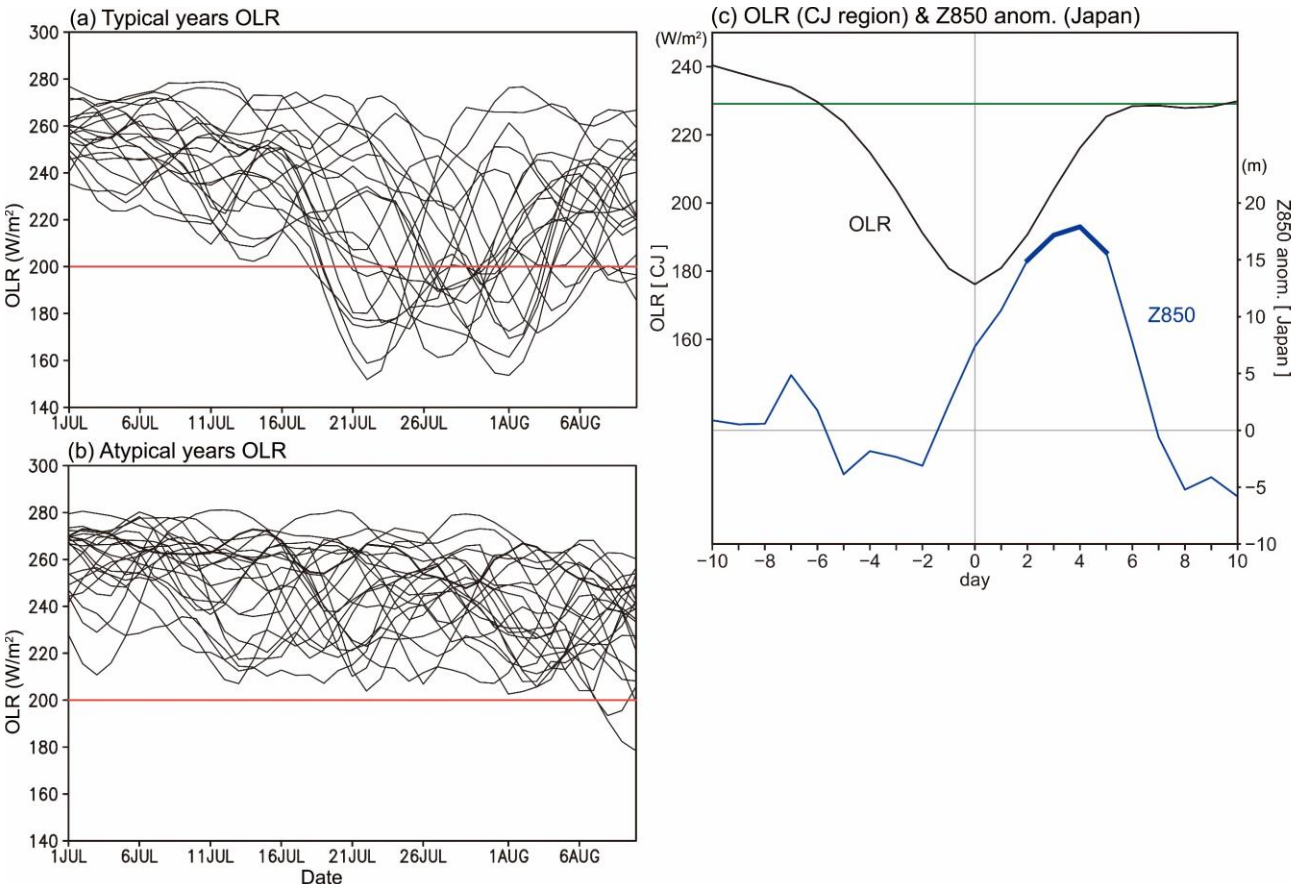


Fig. 2. Time series of (a) typical and (b) atypical CJ years for 5-day running mean OLR averaged over the CJ region (black lines; W m$^{-2}$) from July 1 to August 10. Red lines indicate 200 W m$^{-2}$ OLR. (c) Time series of composite OLR averaged over the CJ region (black line; W m$^{-2}$) and composite 850-hPa geopotential height (Z850) anomaly averaged over the east of Japan [35–45°N, 135–155°E] (blue line; m) for CJ days. A green line denotes the climatological mean OLR for July 20–August 8. Thick lines of Z850 indicate statistical significance at the 95% confidence level of the anomalies.

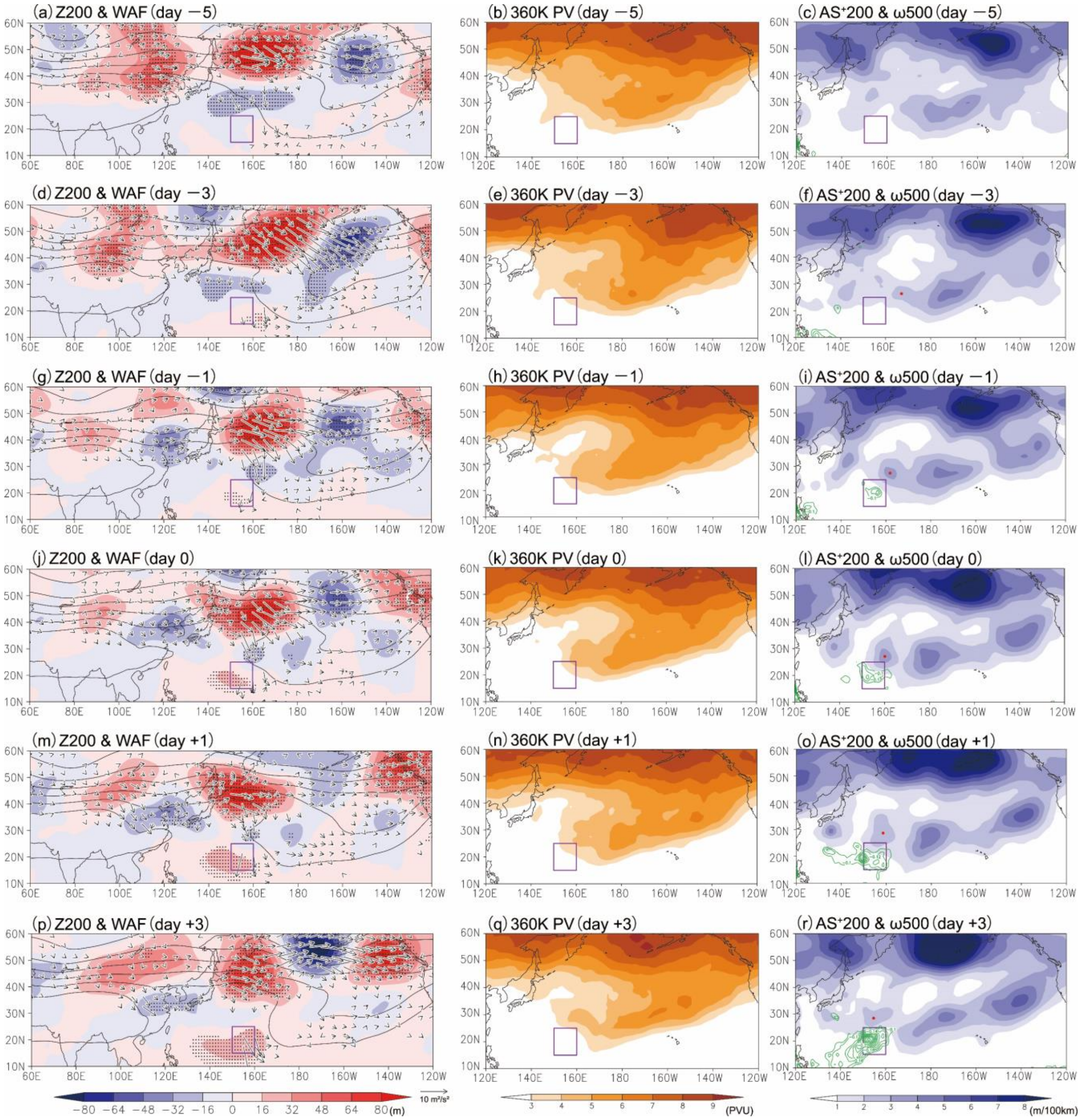


Fig. 3. Composite of (left column) geopotential height (contours; 12000–12500 m, with 100-m intervals), its anomalies (shading; m), and WAF (vectors; $m^2 s^{-2}$) at 200 hPa; (middle column) 360-K PV (shading; PVU); and (right column) AS⁺ of the COL index at 200-hPa (shading; m [100 km] $^{-1}$) and 500-hPa vertical *p*-velocity (green contours; ≤ −0.1 Pa $s^{-1}$, with intervals of 0.2 Pa $s^{-1}$). Red dots represent the centers of a cutoff low contributing to CJ onset. Stippling in the left column indicates statistical significance at

the 95% confidence level of the 200-hPa geopotential height anomalies. (a–c) day −5, (d–f) day −3, (g–i) day −1, (j–l) day 0, (m–o) day +1, and (p–r) day +3. Purple rectangles indicate the CJ region.

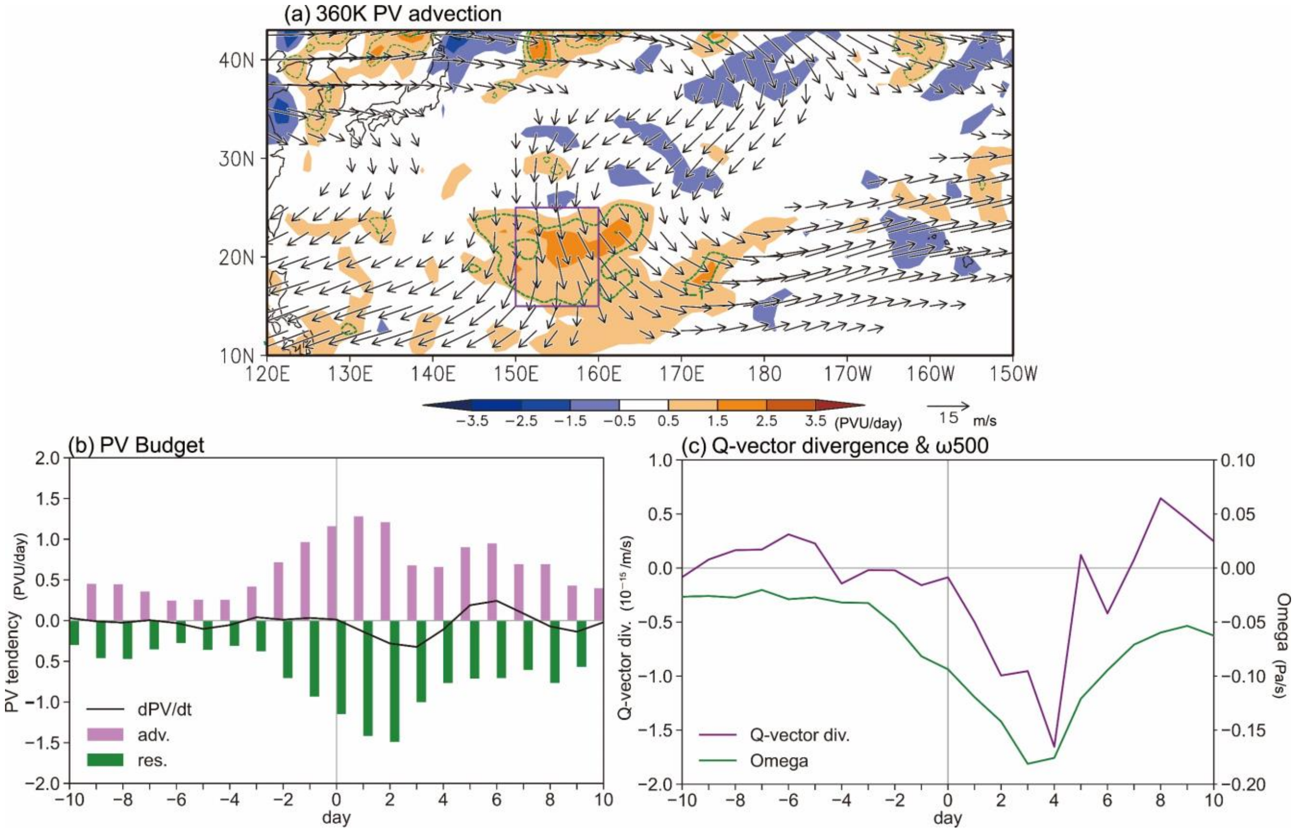


Fig. 4. (a) Advection (shading; PVU day$^{-1}$) and residual terms (contours; < 0 PVU day$^{-1}$) of the PV equation on day 0 at 360 K, based on the composite fields. The contour interval is 1.0 PVU day$^{-1}$. Composite horizontal winds at 360 K are superimposed by vectors (m s$^{-1}$). The purple rectangle indicates the CJ region. (b) Time series of local PV tendency (black line), horizontal advection of PV (magenta bars), and residual term (green bars) at 360 K averaged over the CJ region (PVU day$^{-1}$). (c) Time series of composite anomalous *Q*-vector divergence integrated from 850 to 200 hPa (purple line; $10^{-15}$ m$^{-1}$ s$^{-1}$) and composite vertical *p*-velocity at 500 hPa (green line; Pa s$^{-1}$) averaged over the CJ region.

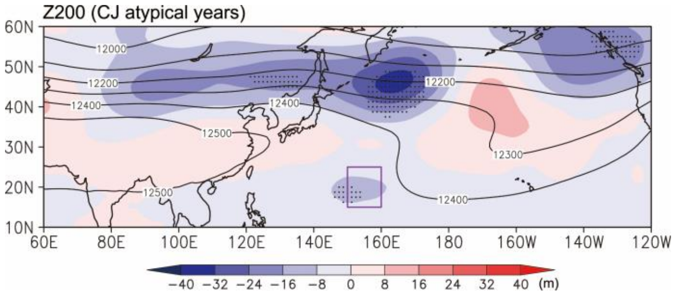


Fig. 5. Composite of 200-hPa geopotential height (black contour; m) and its anomaly (shading; m) in July 20–August 8 for atypical years. Stippling indicates statistical significance at the 95% confidence level. The purple rectangle indicates the CJ region.

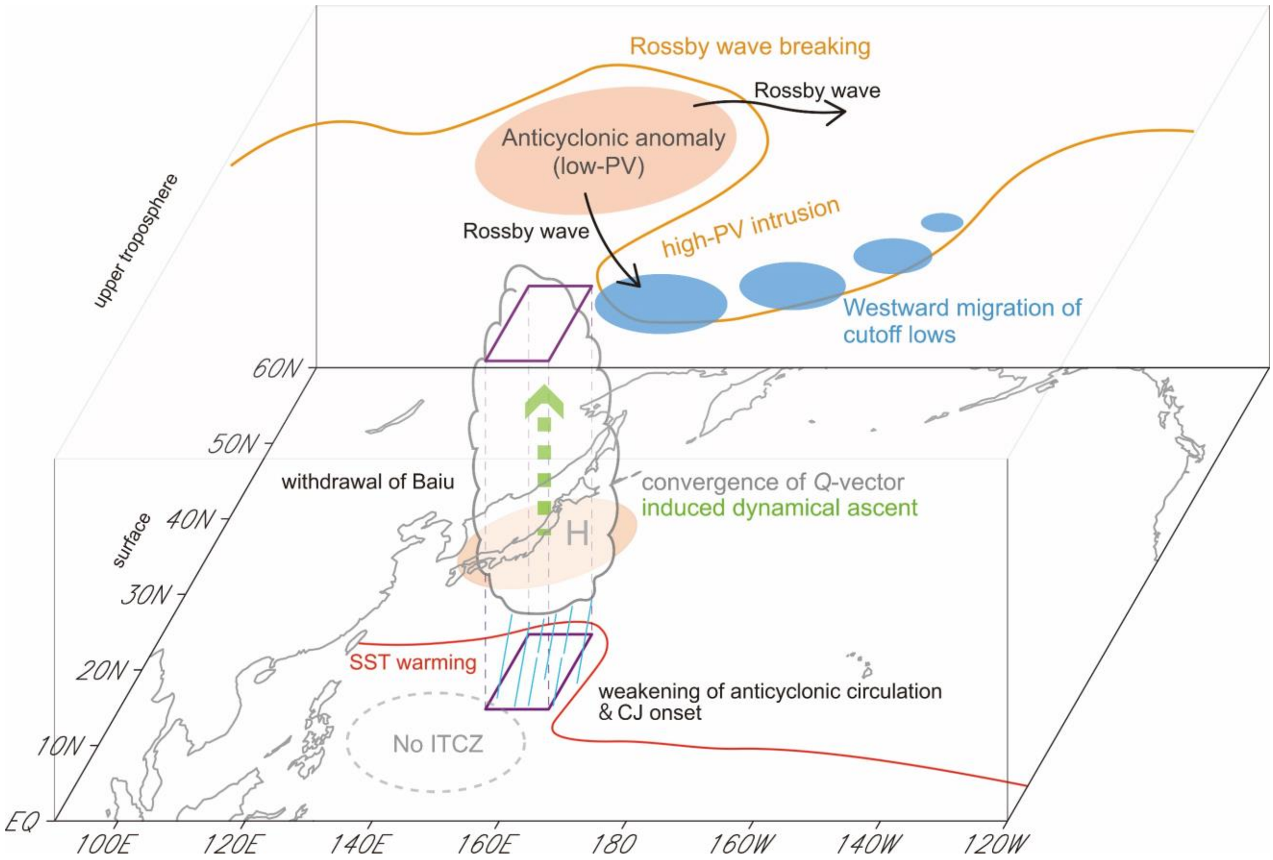


Fig. 6. Schematic illustration of CJ onset mechanisms over the subtropical WNP.

## List of Tables

Table 1 Detected CJ days for typical years (20 years).

| | | | | |
|---|---|---|---|---|
| Aug 1, 1980 | Aug 5, 1986 | Jul 25, 1994 | Jul 23, 2004 | Aug 3, 2016 |
| Aug 1, 1981 | Jul 27, 1988 | Jul 27, 1998 | Jul 29, 2009 | Jul 27, 2017 |
| Jul 27, 1984 | Aug 1, 1989 | Jul 20, 1999 | Aug 1, 2012 | Jul 29, 2018 |
| Jul 22, 1985 | Jul 27, 1990 | Jul 22, 2002 | Aug 4, 2015 | Jul 22, 2021 |